91602
new 82-10

LEGAL NOTICE

This report was prepared by Ontario Hydro and, while effort has been made to assure the accuracy and applicability of the material contained herein, neither Ontario Hydro nor any person acting on its behalf:

(a) makes any warranty, express or implied with respect to the use of any information, apparatus, method or process disclosed in this report or that such use may not infringe privately owned rights; or

(b) assumes any liabilities with respect to the use of, or for damages resulting from the use of, any information, apparatus, method or process disclosed in this report.

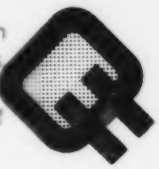

ontario hydro
research division

THE EFFECTS OF MIXED AND RADIAL HYDRIDE MORPHOLOGIES ON THE AXIAL FRACTURE TOUGHNESS OF Zr-2.5Nb PRESSURE TUBE

Report No. 90-44-K

A.C. Wallace
Engineer
Nondestructive and Fracture Evaluation Section
Metallurgical Research Department

ABSTRACT

The effects of hydride morphology on the axial fracture toughness of cold-worked Zr-2.5Nb pressure tube have been investigated as a function of temperature for three different hydride morphologies and hydrogen concentrations. The morphologies were characterized by a parameter referred to as the Hydride Continuity Coefficient (HCC) which provides a measure of the extent to which hydrides are oriented in the axial-radial plane of the pressure tube wall. Hydrides in this orientation are known to reduce fracture toughness. Two mixed morphologies, with hydrides oriented between the radial and circumferential directions, were prepared in undeformed tube sections. These had hydrogen concentrations of 40 and 52 mg/kg and HCCs of 0.04 - 0.21 and 0.13 - 0.25 respectively. The third morphology was prepared in a flattened and stress-relieved strip containing 130 mg/kg hydrogen as radial hydrides with an HCC of 0.73. The fracture toughness of the two mixed morphologies was similar, increasing rapidly with temperature to reach an upper shelf toughness level slightly above 100°C. The fracture toughness of the radially hydrided strip was significantly lower, with brittle fracture observed at all test temperatures below 270°C. Although ductile behaviour was observed at 270°C and 280°C, the maximum load toughness values for these specimens were below the upper shelf level determined previously for other morphologies. In addition, brittle fracture was observed at 275°C and 280°C. From these observations it is concluded that the transition to upper shelf toughness for this morphology is not fully complete until temperatures greater than 280°C are reached.

job	file	date	report no.
83-293-551	826.231	April 10, 1990	90-44-K

90-06106/

ontario hydro
research division

EXECUTIVE SUMMARY

THE EFFECTS OF MIXED AND RADIAL HYDRIDE MORPHOLOGIES ON THE AXIAL FRACTURE TOUGHNESS OF Zr-2.5Nb PRESSURE TUBE

Report No. 90-44-K

A.C. Wallace
Nondestructive and Fracture Evaluation Section
Metallurgical Research Department

Objective: The objective of the work was to investigate the effects of differences in hydride orientation and hydrogen concentration on the fracture toughness of Zr-2.5Nb pressure tube as a function of temperature. Three different morphologies were examined - two mixed and one radial.

Major Results:

1. Mixed hydride morphologies with HCC values below 0.2 and hydrogen concentrations less than 55 mg/kg have only a minor effect on toughness. No effect is observed above about 100°C.

2. The toughness transition for material containing 130 mg/kg hydrogen as radial hydrides (HCC=0.73) begins at about 240°C and is not fully completed at 280°C.

3. The abrupt toughness transition observed at 240°C for morphologies with significant proportions of radial hydride (HCC values greater than 0.4 - 0.5) probably occurs over a wider temperature range than previously thought.

4. For morphologies having predominantly radial hydrides, the temperature at which the abrupt toughness transition is complete increases with higher hydrogen concentrations and HCC values.

Recommendations:

1. Testing should continue to determine the fracture behaviour of morphologies with HCC values between 0.2 and 0.5.

2. Work is required to determine the role of hydride platelet size and coarseness in Zr-2.5Nb fracture. This should provide a better understanding of the mechanism of the toughness transition in material with high concentrations of radial hydride.

3. Similar tests should be repeated for the actual pressure tube geometry.

job	file	date	report no.
83-293-551	826.231	April 10, 1990	90-44-K

TABLE OF CONTENTS

		PAGE
1.0	INTRODUCTION	1
2.0	CONCLUSIONS	2
3.0	RECOMMENDATIONS	2
4.0	EXPERIMENTAL DETAILS	3
4.1	Preparation of Test Morphologies	3
4.2	Characterization of the Morphologies	4
4.3	Test Specimen Preparation	5
4.4	Tensile Tests	6
4.5	Fracture Toughness Tests	7
5.0	RESULTS	8
5.1	Fracture Toughness Parameters	9
5.2	Post-Test Examinations	14
5.2.1	Mixed Morphologies - Tubes 1 and 2	14
5.2.2	Radially Hydrided Strip	17
6.0	DISCUSSION	21
6.1	Transition Behaviour	21
6.2	Initiation Toughness	22
6.3	Geometry Effects	22
ACKNOWLEDGEMENT		23
REFERENCES		24
DISTRIBUTION		last page

ontario hydro
research division

To

Mr. R.W. Patterson
Manager
Chemistry and Metallurgy
Central Production Services
A8 H6

THE EFFECTS OF MIXED AND RADIAL HYDRIDE MORPHOLOGIES ON THE AXIAL FRACTURE TOUGHNESS OF Zr-2.5Nb PRESSURE TUBE

1.0 INTRODUCTION

The effects of zirconium hydride on the fracture toughness of zirconium alloy pressure tubes have been well documented /1-4/. However, while the embrittling effect of hydride platelets oriented in the radial-axial plane has been emphasized, more specific information about the variation of toughness over wider ranges of hydride orientation and hydrogen concentration in Zr-2.5Nb is limited. The results of a systematic study on four different morphologies /5/ have provided some of the required data, but information is still scarce concerning the effects of mixed hydride structures such as those seen in tubes removed from PNGS B Unit 8 /6/ and BNGS A Unit 2 channel X-14 /7/, in which hydrides were oriented between the radial and circumferential planes of the pressure tube. As well, comparatively little information is available on material with very high hydrogen concentrations. Thus, as deuterium levels in operating pressure tubes increase, more detailed fracture toughness data will be required for use in pressure tube fitness for service assessments.

This report summarizes the results of tests performed on three different hydride morphologies that will help to provide some of the missing information. The work was initiated at the request of the Chemistry and Metallurgy Section of Central Production Services (Central Nuclear Services at the time). Additional funding was subsequently obtained from the CANDU Owners Group (COG) for a more comprehensive research program to generate fracture toughness data as a function of temperature for a range of hydrogen concentrations and hydride morphologies in both unirradiated and irradiated material. This work is currently in progress. Further analysis of the results in this report, and comparisons with other data will be included in a future COG report.

2.0 CONCLUSIONS

1. Mixed hydride morphologies with HCC values below 0.2 and hydrogen concentrations less than 55 mg/kg have only a minor effect on toughness. No effect is observed above about 100°C.

2. The toughness transition for material containing 130 mg/kg hydrogen as radial hydrides (HCC=0.73) begins at about 240°C and is not fully completed at 280°C.

3. The abrupt toughness transition observed at 240°C for morphologies with significant proportions of radial hydride (HCC values greater than 0.4 - 0.5) probably occurs over a wider temperature range than previously thought.

4. For morphologies having predominantly radial hydrides, the temperature at which the abrupt toughness transition is complete increases with higher hydrogen concentrations and HCC values.

3.0 RECOMMENDATIONS

1. Testing should continue to determine the fracture behaviour of morphologies with HCC values between 0.2 and 0.5.

2. Work is required to determine the role of hydride platelet size and coarseness in Zr-2.5Nb fracture. This should provide a better understanding of the mechanism of the toughness transition in material with high concentrations of radial hydride.

3. Further work is required to investigate the effects of specimen geometry on the results reported here. The amount that hydrides influence toughness is expected to vary because of the differences in constraint between small specimens and full size pressure tubes.

4.0 EXPERIMENTAL DETAILS

4.1 Preparation of Test Morphologies

Uniform mixed morphologies of hydrides oriented between the radial and circumferential planes were produced in two 500mm long tube sections. Earlier attempts to produce this type of structure in flattened strips of tubing were unsuccessful because of residual stresses that remained even after stress-relieving for 40h at 400°C /5/. A hydride layer was electrolytically deposited on the middle 150mm of the outside surface in a 0.1M sulphuric acid electrolyte at 90°C and a current density of 120 mA/cm^2. Titanium end-caps were electron-beam welded to the ends of the tube sections which were then internally pressurized to 12.5-13 MPa and heated to diffuse in hydrogen from the layer. The first tube was held at 300°C for 160h while the second was held at 265°C for 220h to produce nominal hydrogen concentrations of 60 and 40 mg/kg, respectively. The tubes were cooled at a rate of about 0.9°C/min under a pressure of 12.4 MPa, equivalent to a hoop stress of 160 MPa. Figures 1 and 2 show the morphologies of the first and second tubes, hereafter referred to as tube #1 and tube #2.

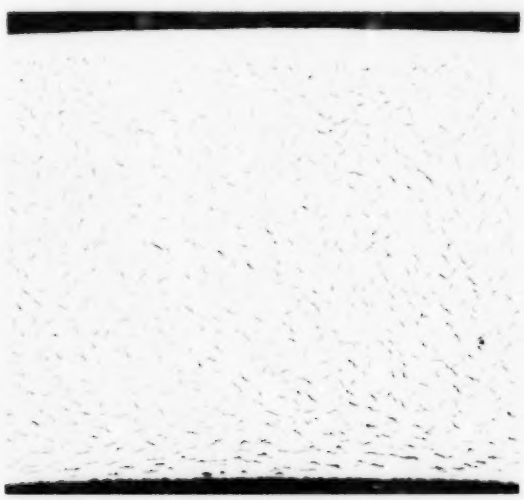

Figure 1: Morphology of Tube #1 (X16)

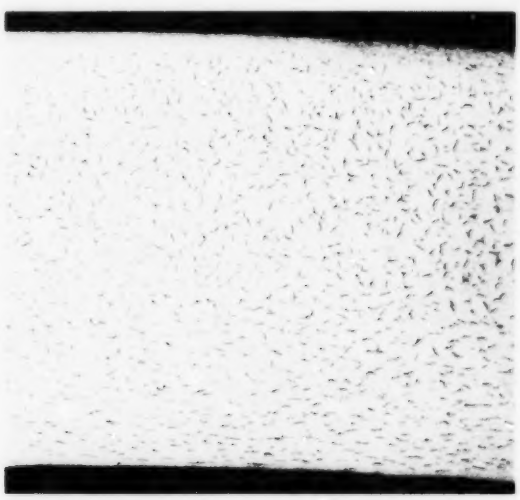

Figure 2: Morphology of Tube #2 (X16)

A third morphology was prepared in a flat strip produced from a flattened and stress relieved ring of pressure tube. A hydride layer was electrolytically deposited on the surfaces under the same conditions described above for the tube sections. The strip was mounted in a tensile machine and heated for 20h at 350°C to diffuse in hydrogen to a nominal concentration of 100 mg/kg. A 350 MPa stress was applied during cooling at 1.5°C/min, producing the radial hydride morphology shown in Figure 3.

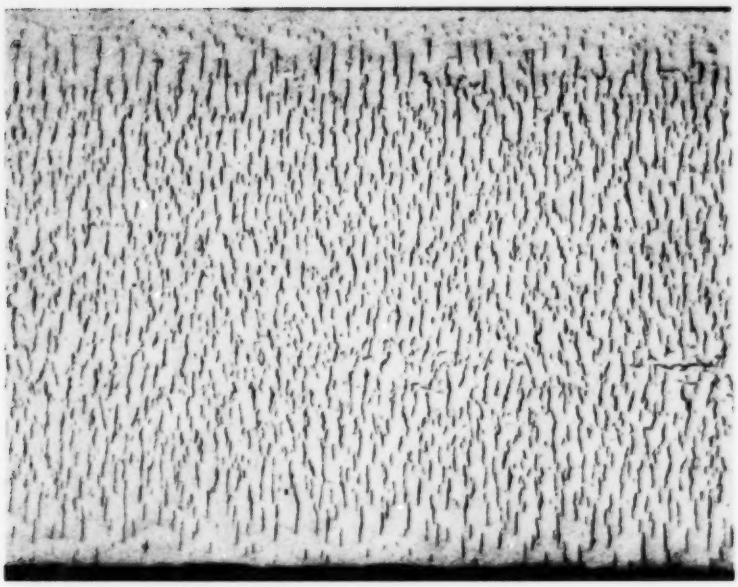

Figure 3: Morphology of flat strip (X20)

4.2 Characterization of the Morphologies

The morphologies obtained in the tubes and the strip were essentially as intended. Figures 1 and 2 show that the hydride orientation in the two tubes lies between the radial and circumferential planes and is uniform through the outer two-thirds of the wall. The zone of circumferential hydride near the inside wall results from residual stresses from tube fabrication. Figure 3 shows the structure of fully radial hydrides obtained in the strip. All three structures show a hydride depleted zone extending about 0.2mm below the surface. This is a commonly observed feature /5,8/ of morphologies prepared in this fashion. The reasons for it are not clear, but may be related to an increased oxygen concentration in the zone.

Hydrogen analysis was performed using a hot vacuum extraction technique. The hydrogen concentration of the second tube was close to the target value, while that of the first tube was lower than expected. This is probably a result of too short a hold time at the diffusion temperature. The concentration of the strip was higher than expected, possibly the result of errors in temperature measurment.

The hydride morphologies were characterized by a parameter referred to as the Hydride Continuity Coefficient (HCC), which measures the degree to which hydrides are oriented in the radial-axial plane of the pressure tube /9/. The HCC can have a value between 0 and 1 with a low value corresponding to a morphology with only a few small hydrides present, or hydrides oriented mainly in the axial-circumferential plane (the most common form). A high HCC is indicative of a high degree of hydride reorientation to the radial-axial plane, and low toughness over a wide temperature range /4,5/. The results reported here were obtained by the method in /9/ with some minor modifications. Measurements were performed on a 10mm wide radial strip on a 100X micrograph of the radial-circumferential plane. The entire sample thickness was considered, with the exception of the hydride depleted zones near each surface. It should be noted that since HCC measurements are performed on micrographs taken at room temperature, the values obtained may differ from from the true values at elevated temperature, where much of the hydride present may have dissolved. However, in-house investigations suggest that this effect is minor, and that partially dissolved hydrides tend to become thinner and less continuous rather than shorter. The HCC is dependent on the projected lengths of hydrides, which should not be sensitive to changes in platelet coarseness. The results of hydrogen analysis and HCC measurements for the three morphologies are summarized in Table 1.

Table 1: Hydrogen Concentration and HCC Measurements

Material	[H] (mg/kg)	HCC
Tube #1	48 - 54	.13 - .25
Tube #2	33 - 44	.04 - .21
Strip	130	.73

4.3 Test Specimen Preparation

Twelve compact tension C(T) specimens were machined from each hydrided tube section. Eight transverse tensile specimens were prepared from tube #1. These specimens were of the type developed at AECL-WNRE for testing of pressure tubes removed from reactor /10/. The C(T) specimens retain a small amount of tube curvature, but this has been demonstrated to have no significant effect on fracture toughness results /11/. The nominal width, W, of these specimens is 17mm, with the other in-plane dimensions in the proportions specified in ASTM E399. An exception is the spacing of the pin holes, which are positioned closer together to minimize the bending effect due to the specimen curvature. Analysis has shown that this does not significantly affect the stress intensity factor calibration in the applicable crack length range /12/. The tensile specimens have a rectangular cross-section and are ground flat to remove curvature. Twelve C(T) specimens and six transverse tensile specimens were machined from the flat strip. The C(T) specimens had the same planar dimensions as the curved specimens machined from the tubes. The tensile specimens had a round cross-section with the same dimensions as those tested in /5/.

4.4 Tensile Tests

Duplicate specimens from Tube #1 were tested at room temperature, 175°C and 240°C at a strain rate of 1×10^{-3}/s. Specimens from the strip were tested at six temperatures from room temperature to 285°C at a strain rate of 4×10^{-4}/s. Before testing, the specimens were held at the test temperature for a time sufficient to allow the hydride to dissolve to the equilibrium concentration. Results are summarized in Table 2. Figure 4 plots the flow stress, taken as the average of the yield stress and the UTS, for both sets of specimens as a function of temperature. There is essentially no difference in the strength properties, although the radially hydrided strip showed significantly less ductility below 100°C.

Table 2: Tensile Properties

	T(°C)	σ_{ys}(MPa)	UTS(MPa)	% Tot.El.	% R.A.
Tube #1:	23	840	855	15.3	48.1
	175	648	676	14.5	67.1
	240	584	621	12.3	67.9
Strip:	23	820	820	0.3	1.2
	100	737	744	9.8	32.5
	172	659	671	15.9	69.7
	225	608	624	14.7	70.9
	280	578	595	14.7	73.8
	285	574	597	14.2	74.4

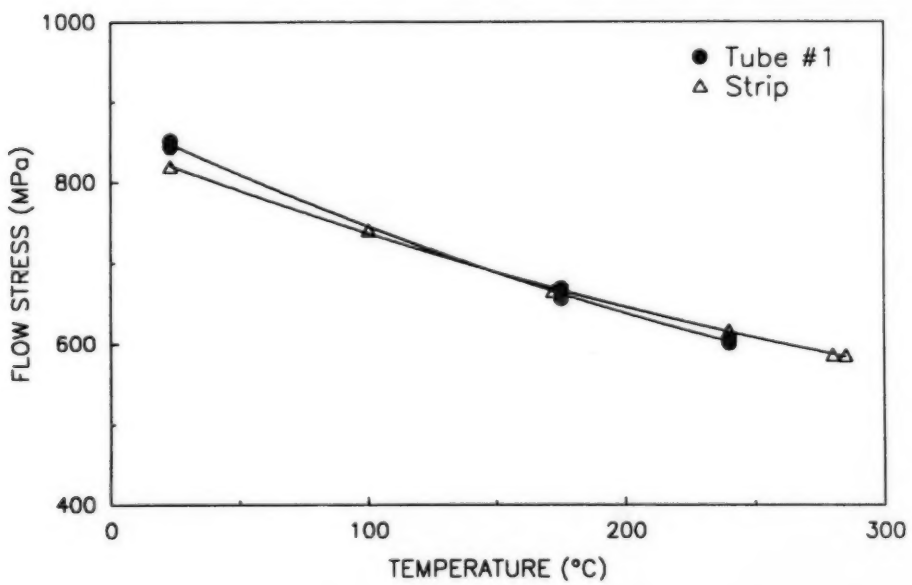

Figure 4: Comparison of transverse flow stress for tube #1 and Strip

4.5 Fracture Toughness Tests

Prior to testing, the C(T) specimens were fatigue precracked at an initial maximum stress intensity factor, K_I, of 13 MPa$\sqrt{m}$ (R=0.1), which was gradually reduced to a final value of 8 MPa$\sqrt{m}$.

Testing was performed in accordance with ASTM standard test method E1152 for determining J-R curves, with crack extension measured by the direct current potential drop technique /13/, instead of the elastic compliance method. Electrical current leads were attached near the top and bottom of the front face of the specimen. Potential leads of 0.75mm diameter zirconium wire were spot-welded to opposite sides of the crack mouth, as close as possible to the crack plane. A constant current of 1 ampere was applied to the specimen and the voltage across the crack mouth was amplified 10000X.

A computer-based data acquisition system was developed to record load, displacement and amplified potential drop voltages at regular intervals. Tests were performed in displacement control at a rate of about 0.01mm/s. Displacement was measured by attaching a clip gauge to the clevises along the load line and correcting for the deflection of the loading pins. After testing, the extent of any stable crack extension was marked by heat tinting or anodizing in an oxalic acid solution. Initial and final crack lengths were calculated by computer from a digitized image of the fracture surface. Physical crack extension was determined assuming a linear variation of potential drop voltage with crack length /13/. J-R curves were developed according to the method in ASTM standard E1152. Brittle specimens were analysed according to ASTM standard test method E399.

Specimens from the tube sections were tested at room temperature, 75, 100, 175 and 240°C, while those from the strip were tested at room temperature, 172, 240, 252, 260, 265, 270, 275 and 280°C. Specimens were held at the test temperature prior to testing, for sufficient time to ensure dissolution of the hydride to the equilibrium concentration. Nominal hold times of 24h at 75°C and 100°C, 17h at 175°C, 4h at 240°C, 3h at 260°C and 2h at 270, 275 and 280°C were chosen based on information in /14/.

5.0 RESULTS

The test results are summarized in Table 3 and in figures 5, 6 and 7. An explanation of the toughness parameters listed in Table 3 and plotted in Figures 6 and 7 is provided in section 5.1. Section 5.2 summarizes the findings of fractographic examinations of the specimens.

In general, the results show only minor differences in the fracture toughness of tubes 1 and 2. At temperatures below 100°C, the toughness of tube #1 appears to be slightly lower. This can be attributed to its higher hydrogen content, which on average is about 10mg/kg more than tube #2. At higher temperatures this is apparently not enough to produce any significant effect. For both tubes, the transition to the upper shelf toughness limit appears to be complete somewhere between 100°C and 175°C.

The toughness of the radially hydrided strip is essentially constant from room temperature to above 240°C. At about 240°C the toughness enters a transition region. Here toughness increases rapidly, but full upper shelf behaviour does not appear to have been reached at 280°C.

Figure 5 compares typical J-R curves from tubes 1 and 2 from room temperature to 240°C. No J-R curves could be obtained from the strip in this temperature range.

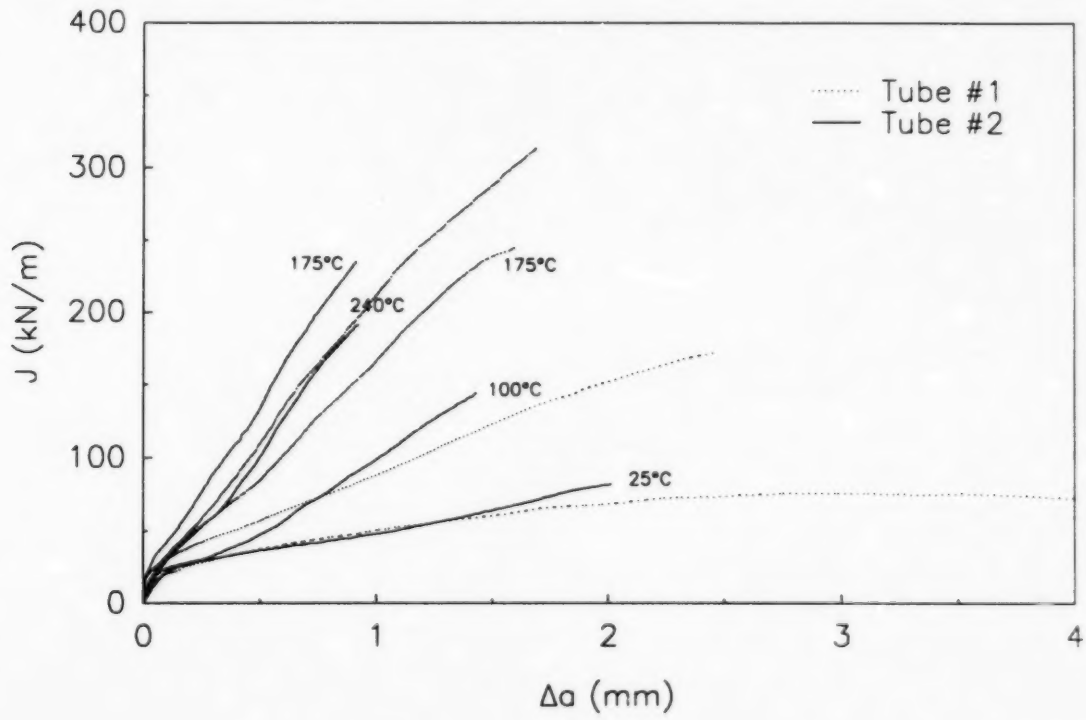

Figure 5: Comparison of J-R Curves from Tubes 1 and 2.

5.1 Fracture Toughness Parameters

Table 3 summarizes the test results, giving test temperatures, toughness parameters, and, where measured, the hydrogen concentrations and HCC values for each specimen. Two toughness parameters, K_Q and K_{max}, are given in the table, and are defined as follows.

The parameter K_{max} is simply the value of the opening mode linear elastic stress intensity factor, K_I, evaluated at the maximum load attained during the test. For brittle specimens, K_{max} is defined according to ASTM E399 as

$$K_{max} = [P_{max}/(BW^{1/2})]f(a/W) \qquad (1)$$

where: P_{max} = maximum load applied during test,
B = specimen thickness (4.2mm),
W = specimen width (17mm), and

$$f(a/W) = \frac{(2+a/W)(0.886+4.64a/W-13.32(a/W)^2+14.72(a/W)^3-5.6(a/W)^4)}{(1-a/W)^{3/2}}.$$

For ductile specimens, that is, those exhibiting stable crack extension during the test, K_{max} is determined from the value of J at maximum load, J_{max}, using the plane stress relation

$$K_{max} = (EJ_{max})^{1/2} \qquad (2)$$

where E is Young's modulus. Here J is defined as the sum of an elastic component, J_{el}, and a plastic component, J_{pl}. J_{el} is defined as

$$J_{el} = \frac{K^2(1-\nu^2)}{E} \qquad (3)$$

where ν = Poisson's ratio, and K is defined in (1). The plastic component is defined as

$$J_{pl(i)} = [J_{pl(i-1)} + (\eta_i/b_i)\{A_{pl(i)} - A_{pl(i-1)}\}/B_N][1 - \gamma_i\{a_i - a_{(i-1)}\}/b_i] \qquad (4)$$

where: $\eta_i = 2.0 + 0.522\ b_i/W$, and
$\gamma_i = 1.0 + 0.76\ b_i/W$.

The subscript i refers to a given point (P_i, δ_i) on the specimen load vs. displacement record, and the quantity $A_{pl(i)}$-$A_{pl(i-1)}$ is the increment of plastic area under the load vs. displacement record, between lines of constant displacement at points i-1 and i.

The parameter K_Q provides an estimate of initiation toughness. For brittle specimens this corresponds to the value of K_{IC} or K_Q as it would be defined in ASTM E399. In most cases this will be the same as K_{max}. For those specimens that exhibit "pop-ins" followed by further load increases prior to instability, K_Q corresponds to the pop-in K value. For those specimens that show non-linear load-displacement behaviour prior to instability, K_Q is defined by the point of intersection of the load displacment curve and the secant drawn at 95% of the initial slope. For ductile specimens, K_Q is determined from the J_{IC} or J_Q value as defined in ASTM E813, except that J_Q is determined by the intersection of the actual J-R curve and a line drawn parallel to and offset 0.2mm from the blunting line, rather than using a power-law fit to the curve. (In practice, this difference is negligible.) The J values are converted to K values using equation (2).

Table 3 - Summary of Fracture Toughness Test Data

Spec.	[H] (mg/kg)	HCC	Temp. (°C)	K_Q (MPa m)	K_{max} (MPa m)	CCL (mm)	P_m/P_L
Tube #1							
1		0.13	23	52.8	60.8	50.4	0.51
2			23	50.2	61.1	45.0	0.52
3			23	54.6	59.9	43.4	0.58
10	48	0.20	75	50.2	71.9	47.3	0.84
11			75	48.0	74.8	59.0	0.75
9	49		100	64.5	112.8	68.0	1.07
7			175	72.0	111.2	76.5	1.12
8	54		175	82.4	133.5	87.8	1.07
5			240	82.1	118.2	80.2	1.08
6			240	74.6	109.3	80.3	1.15
Tube #2							
A1		0.04	23	54.9	80.4	54.8	0.76
C1		0.10	23	52.2	81.9	56.5	0.89
D2			23	51.3	69.9	42.4	0.77
D3		0.21	23	50.3	68.9	42.2	0.73
A2	40		100	64.6	113.8	76.5	1.04
C2	44		100	53.6	106.6	67.8	0.97
A3	38		175	88.2	123.7	78.8	1.08
C3	44		175	70.4	115.0	74.2	1.05
B1	33		240	70.3	110.1	71.6	1.14
D1			240	78.0	111.1	73.9	1.10
Strip							
1	130	0.73	23	20.7	26.6	12.8	0.25
2			173	22.6	27.0	14.4	0.30
3			240	36.9	36.9	27.3	0.50
4			240	35.2	59.7	24.3	0.78
5			252	33.3	62.9	23.0	0.85
7			260	22.2	32.7	14.0	0.55
8			265	25.8	39.7	17.1	0.57
6			270	30.4	89.9	64.4	1.09
9			270	27.9	82.0	58.8	1.09
10			275	40.0	47.6	27.6	0.72
11			280	41.7	46.5	28.6	0.68
12			280	44.8	93.9	61.1	1.12

Figures 6 and 7 plot the parameters K_Q and K_{max} against temperature for both tubes and the hydrided strip. The results of tests performed on as-received material are included on the graphs for comparison.

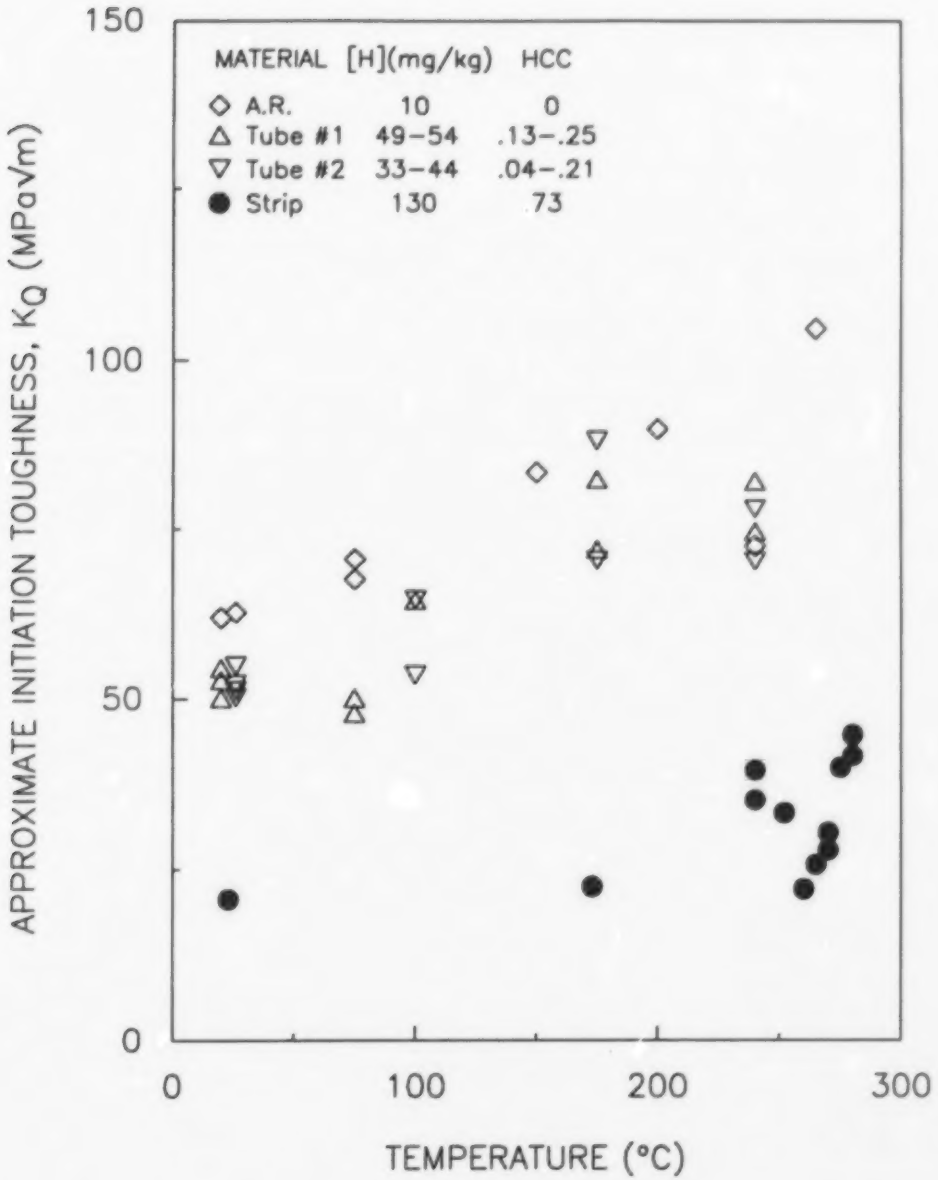

Figure 6: Initiation Toughness, K_Q, vs. Temperature

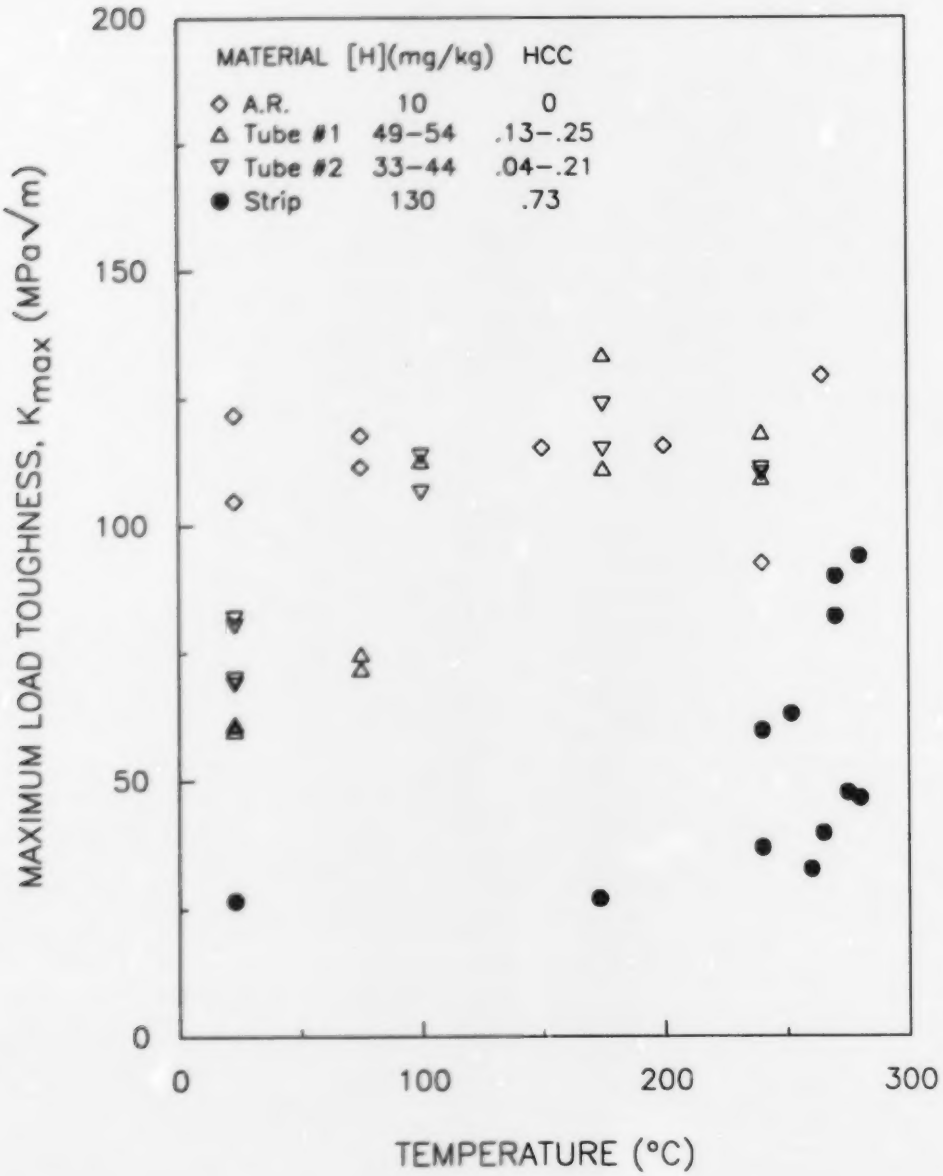

Figure 6: Maximum Load Toughness, K_{max}, vs. Temperature

The second last column in Table 3 gives the critical crack length (CCL), which may be defined as the maximum length of a through-wall axial crack that would be stable for a given set of conditions. For ductile specimens, CCL is evaluated from the tangency of the experimental J-R curve and the theoretical crack driving force curve obtained from Kiefner et. al. /15/, which has the form

$$J = \frac{8a\sigma_f^2}{\pi E} \ln \frac{\sec(\pi M \sigma_h)}{2\sigma_f} \qquad (5)$$

where:
- $2a$ = the axial crack length
- σ_f = the material flow stress $(\sigma_{ys} + UTS)/2$
- σ_h = the nominal hoop stress in the tube
- $M = [\,1 + 1.255(a^2/Rt) - 0.0135(a^2/Rt)^2]^{1/2}$
- R = the tube inside radius, and
- t = the tube wall thickness.

The procedure for evaluating CCL is explained in more detail in /16/. The values in Table 3 were determined from a computer algorithm that automatically determines tangency. The crack driving force curve in equation (5) was calculated for a hoop stress of 130 MPa (pressure = 10MPa, R = 52mm, t = 4mm). For brittle specimens, CCL was determined by converting the K_Q values from Table 3 to J values, substituting them into equation (5) and solving iteratively for a. This is slightly more conservative than using the maximum load K values but is used because the behaviour following an initiation event is uncertain for a load controlled situation.

The last column in Table 3 gives the ratio of the maximum load attained during the test to the theoretical plane stress limit load, calculated as follows /17/.

$$P_L = 1.071\eta B b \sigma_f \qquad (6)$$

where:
- B = thickness
- b = uncracked ligament
- σ_f = flow stress
- $\eta = [(2a/b)^2 + 2(2a/b) + 2]^{1/2} - [2a/b + 1]$
- a = crack length

Comparison of the values in this column with other values in Table 3 and Figures 5 and 6 reveals that the attainment of the upper shelf toughness level is associated with P_m/P_L values approaching 1.0. This behaviour was noted earlier by Simpson /18/, and indicates that the test specimen has attained limit load and is failing by plastic collapse. The J-R curve developed beyond this point is therfore geometry dependent.

5.2 Post-Test Examinations

5.2.1 Mixed Morphologies - Tubes 1 and 2

Examination of fracture surfaces by scanning electron microscopy revealed features consistent with the differences in toughness of tubes 1 and 2. Figure 8 shows the fracture surface of tube 1 specimen 3 tested at room temperature. The fatigue precracked zone is nearly indistinguishable from the region of final fracture, and both zones are characterized by flat facets lying parallel to the fracture plane indicating the presence of radial hydrides. Figure 9 shows these features in more detail in the region ahead of the fatigue precrack. Also visible are a number of dark fissures penetrating the surface which are the result of splitting of circumferential hydrides. In between these features are zones of ductile voids and regions of step-wise fracture angled at about 45° to the surface. The latter features are believed to result from the fracture of mixed hydrides oriented between the radial and circumferential planes.

Figure 8: Fracture Surface of Tube 1 Specimen 3, Tested at 23°C.

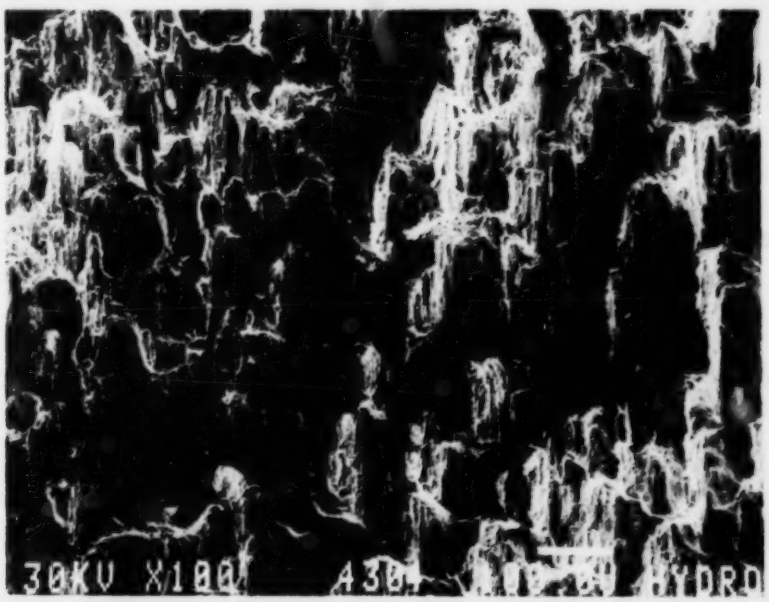

Figure 9: Detail of Region Ahead of Precrack in Figure 7. (X100)

Figure 10 shows the fracture surface of specimen A1 from tube 2, which was also tested at room temperature. The much smoother precrack region is immediately noticeable, and while some parallel facets are visible, they appear smaller and less numerous than those in Figure 8. In contrast, specimen A1 has more perpendicular fissures and zones of ductile voids, as can be seen in Figure 11. The step-wise zones seen in Figure 9 are also present here, but to a lesser extent. These differences reflect the lower values of hydrogen concentration and HCC measured for tube 2. As Figures 1 and 2 show, tube 2 has more circumferential hydride.

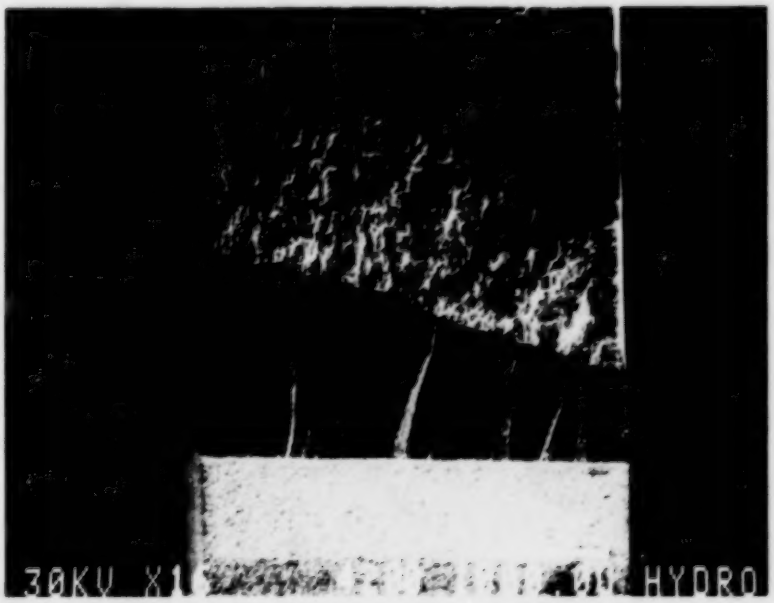

Figure 10: SEM Photograph of Tube 2 Specimen A1 Tested at Room Temperature (X16)

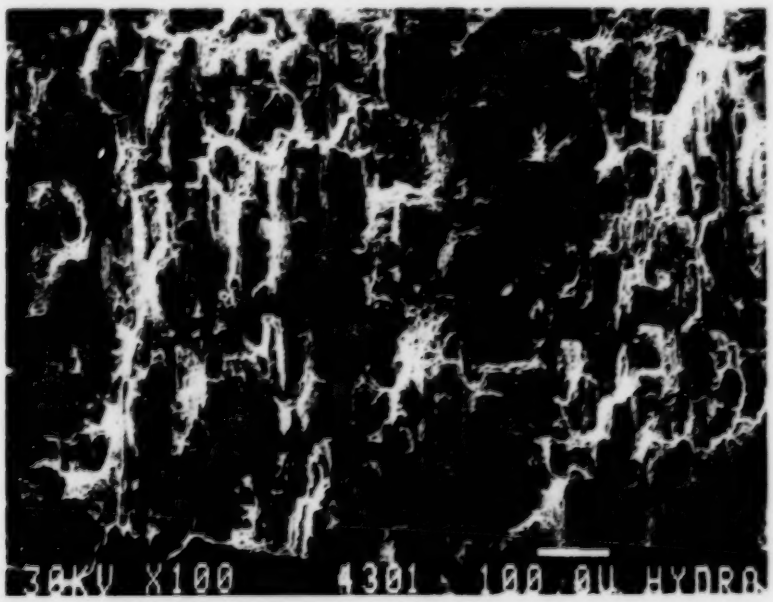

Figure 11: View of Region Ahead of Precrack in Figure 10 (X100)

At higher temperatures, the stable crack growth region of the fracture surfaces is dominated by dimples and elongated furrows as shown in Figure 12. The furrows reflect the elongated grain texture of the pressure tube and are probably the result of ductile void nucleation along the α_{Zr} - β_{Nb} grain boundaries, or at second phase particles such as carbides. The propagating crack tunnels up the mid-section of the specimen and extensive deformation occurs on the outside surfaces, which neck inward. The progression of surface necking with increasing test temperature is shown in Figure 13 which shows 4 specimens from tube 1 which were tested at: a) 23°C; b) 100°C; c) 175°C, and; d) 240°C. The angle of the deformation ahead of the crack-tip is seen to increase with test temperature. The observation that this angle is the same for the specimens tested at 175°C and 240°C is consistent with the earlier observation that the transition to upper shelf toughness is complete below this temperature.

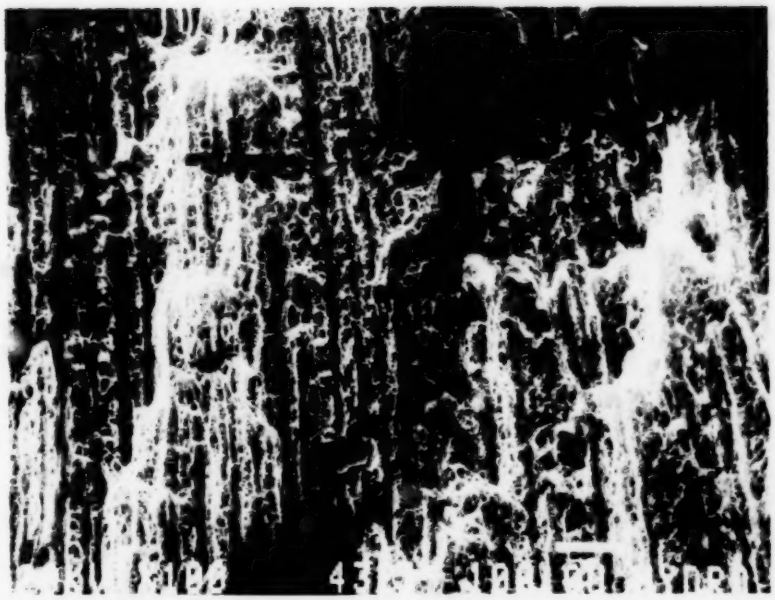

Figure 12: Fracture Surface of Tube 2 Specimen A3 Tested at 175°C (X100)

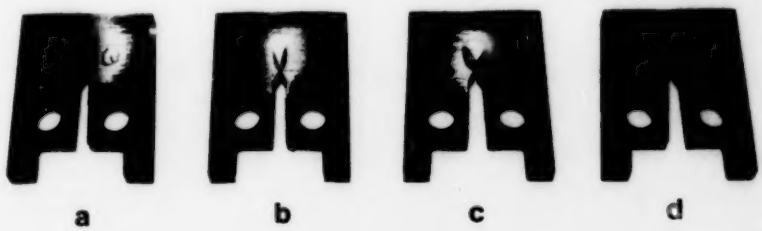

Figure 13: Appearance of Specimens from Tube 1 After Testing

5.2.2 Radially Hydrided Strip

The fracture surfaces of the specimens from the radially hydrided strip were examined to investigate the toughness transition that occurs between 240 and 280°C. Specimens 1, 2, 3, 7, 8, 10 and 11 were all brittle, exhibiting essentially linear load-displacement curves followed by unstable rupture. Figure 14 shows the fracture surface of specimen 8, tested at 265°C. The surface consists entirely of flat cleavage facets from fracture through the radial hydrides. Fracture between individual platelets is presumably by ductile tearing, but these zones are too small to resolve at this magnification. Figure 15 shows the interface between the fatigue precrack and the cleavage fracture region at the mid-section of specimen 8. There are effectively no ductile fracture features to be seen, with the exception of a bright inter-hydride ridge disappearing off the top of the micrograph.

One of the brittle specimens, number 11, tested at 280°C, showed evidence of a small amount of ductility prior to unstable fracture. On this specimen, small isolated regions of elongated furrows and voids, similar in appearance to the structure in Figure 12, could be seen spread out along the interface between the fatigue precrack and the brittle fracture region.

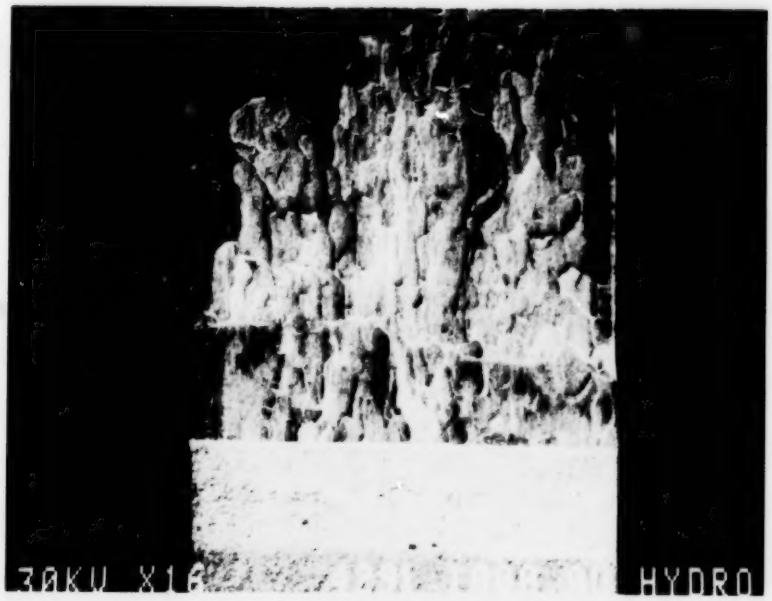

Figure 14: SEM Micrograph of Strip Specimen 8, Tested at 265°C (X16)

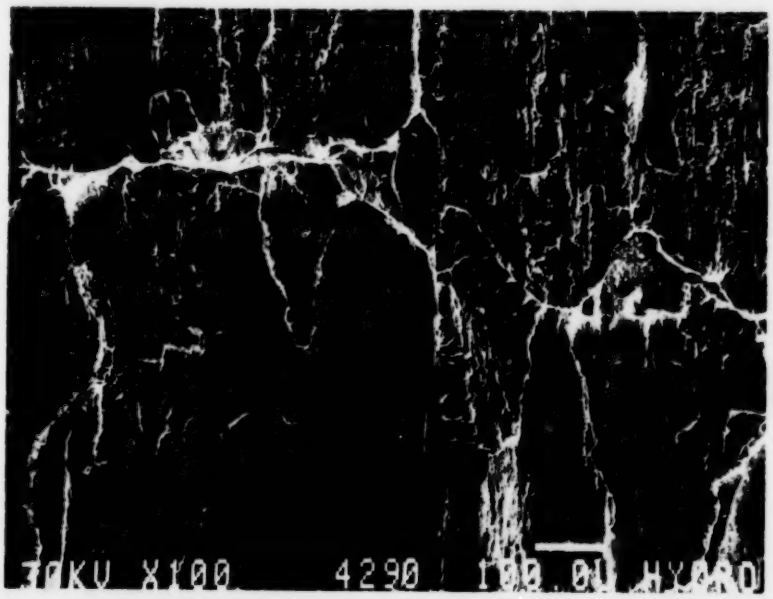

Figure 15: Interface Between Fatigue Precrack and Unstable Fracture Zone in Specimen 8 (X100)

This feature was more evident on the fracture surfaces of specimens 4 and 5, tested at 240°C and 252°C. These specimens also failed in a brittle manner, but with significant nonlinearity in the load - displacement record prior to failure. Figure 16 shows the fracture surface of specimen 4. Clearly, the interface between the fatigue precrack and the final failure is characterized by some ductile fracture features. These are shown in more detail in Figure 17 which shows a small region of dimples and furrows, similar to the ductile features shown previously (Figure 12).

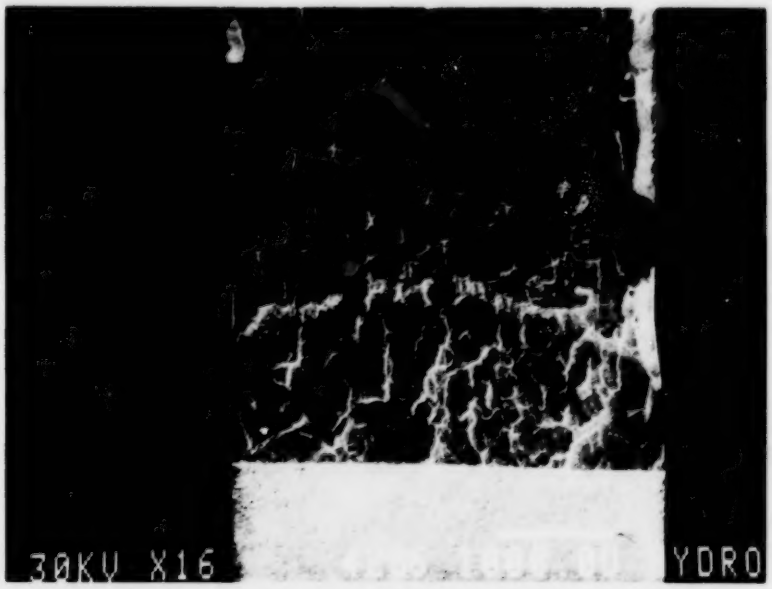

Figure 16: SEM Micrograph of Specimen 4 Fracture Surface (X16)

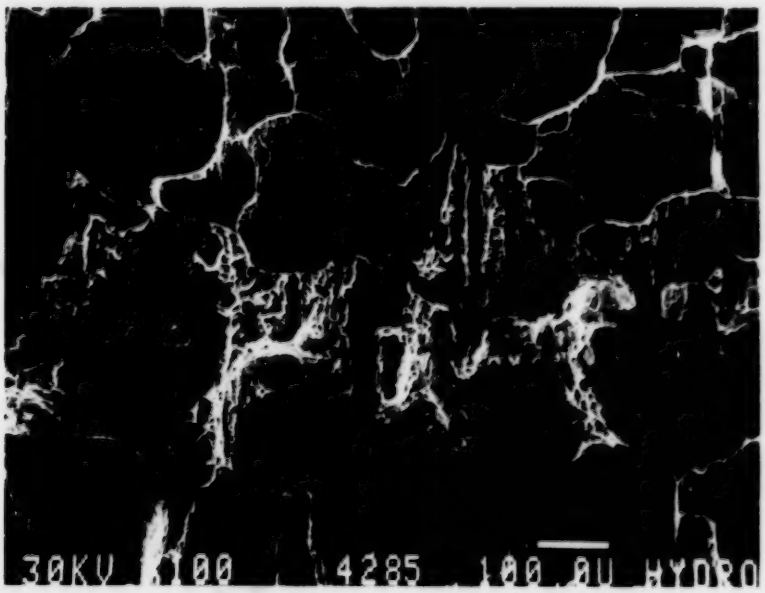

Figure 17: Magnified Image of Region Ahead of Fatigue Precrack in Specimen 4 (X100)

Specimens 6 and 12, tested at 270 and 280°C exhibited ductile behaviour with stable crack extension. The fracture surface of Specimen 6 is shown in Figure 18, which shows that the crack has propagated by tunnelling up the centre of the specimen, with significant necking occurring on the surfaces. Figure 19 shows the region ahead of the precrack in specimen 6, revealing small stretched zones leading into ductile dimples and furrows.

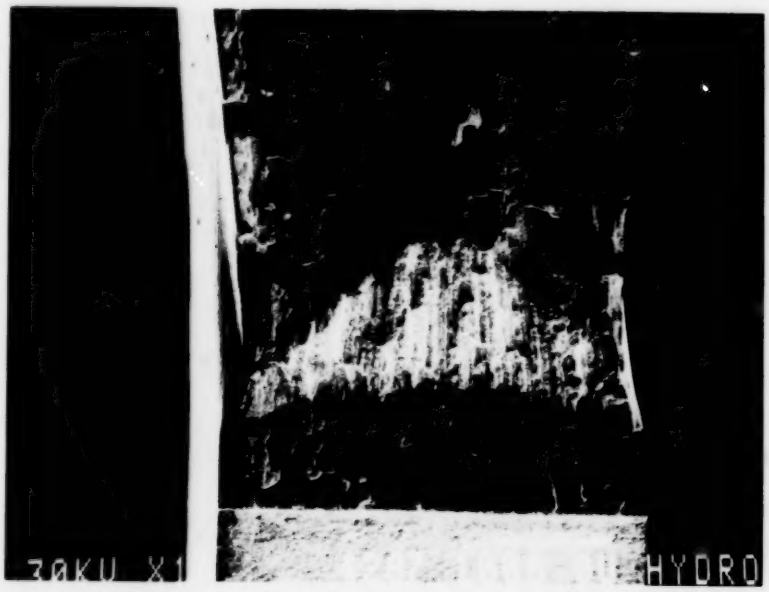

Figure 18: SEM Micrograph of Fracture Surface of Specimen 6, Ductile at 270°C (X16)

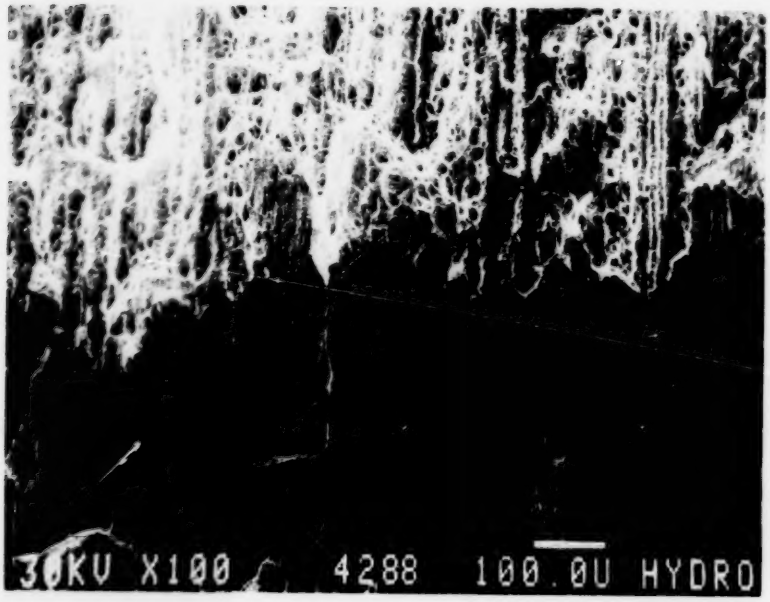

Figure 19: Magnified View of Features Ahead of Precrack in Specimen 6 (X100)

The behaviour of specimen 9, tested at 270°C, was unusual. A brittle pop-in was observed at a load of about 1.75 kN, followed by stable, ductile crack growth. Figure 20 shows the specimen fracture surface, which shows a brittle fracture region extending about 1 mm ahead of the fatigue precrack, followed by a ductile fracture zone. Some necking is apparent adjacent to the region of ductile growth.

Figure 21 shows the interface between the brittle pop-in region and the ductile fracture zone. There is evidence of a small amount of blunting ahead of the arrested crack, preceding the transition to a ductile fracture mode.

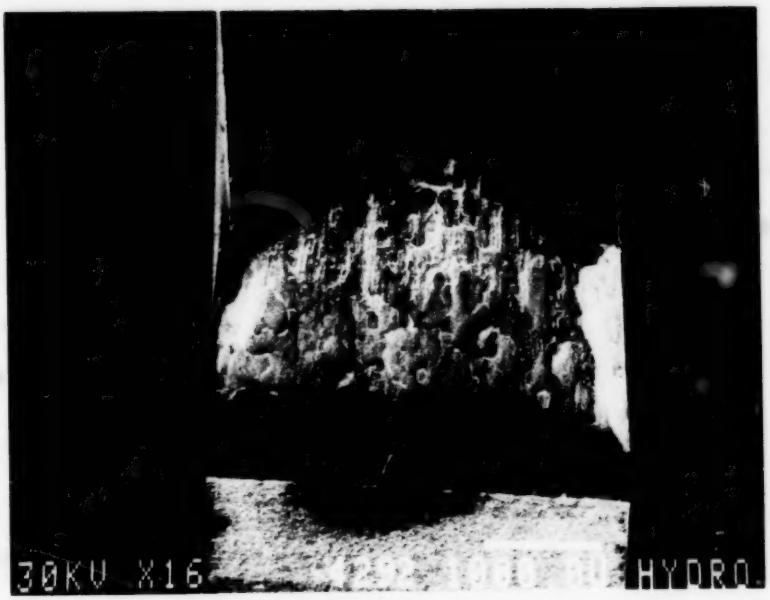

Figure 20: SEM Micrograph of Fracture Surface of Specimen 9 Tested at 270°C (X16)

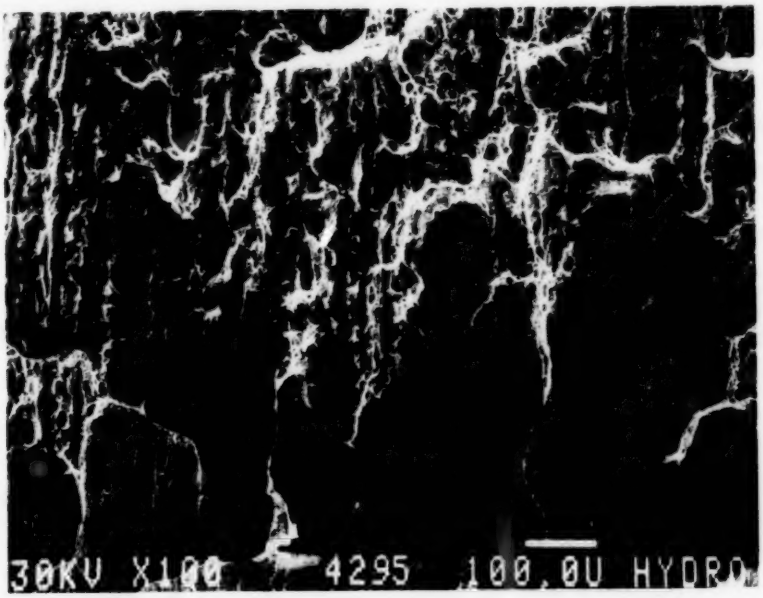

Figure 21: Interface Between Brittle and Ductile Fracture Zones of Specimen 9 (X100)

6.0 DISCUSSION

6.1 Transition Behaviour

In general, the results demonstrate the well known influence of hydride orientation on Zr-2.5%Nb fracture toughness. While the mixed morphologies in tubes 1 and 2 produce only a moderate reduction in toughness at temperatures below about 100°C, the radial-axial orientation of the strip dramatically embrittles the material at temperatures as high as 280°C. Since the strip contained 2-3 times the amount of hydrogen as the two mixed morphologies, it is more reasonable to compare the toughness of tubes 1 and 2 with radial morphologies having a lower concentration. This was done in reference /19/ which compared the toughness of tubes 1 and 2 with the results from /3/ and /5/ for radial morphologies with hydrogen concentrations from about 50-80 mg/kg and HCC values from 0.5-0.7. These results showed similar embrittlement at low temperatures but suggested a rapid transition to upper shelf toughness at about 240°C. However, no tests were performed between 175 and 240°C or above 240°C. In light of the results from the 130 mg/kg strip given here, it seems likely that this earlier transition may occur over a wider temperature range than was earlier believed.

As discussed in /19/, the reasons for the transition are most likely related to a loss of specimen constraint and the partial dissolution of the hydrides as temperature increases. Constraint loss results from a reduction of the material flow stress and an increase in the crack tip plastic zone size, as shown in Figure 13. This corresponds into a reduction of the degree of triaxiality of the crack tip stress state. Simpson /20/ and Puls /21/ have shown that a triaxial stress state encourages hydride fracture. In /20/ it was postulated that fracture of individual hydrides is dependent upon the nucleation and growth of internal flaws. This will be dependent on the stress normal to the hydride platelet and on the hydride size, both of which decrease at higher temperatures. As hydrides dissolve, they become thinner and less continuous. It then becomes more difficult to nucleate a critical flaw within a hydride, particularly if nucleation occurs at pre-existing microcracks. On this basis it would be reasonable to expect that toughness in the transition regime would be a statistically distributed quantity, and that the transition to upper shelf behaviour would occur gradually over a finite temperature range.

This model can also be used to explain the apparent upwards shift in the transition temperature with increasing hydrogen concentration. The results in /3/ and /5/ indicate that the transition is nearly complete at 240°C, while the results for the strip reported here suggest that the transition is not complete until at least 280°C. The main difference between the materials is the higher hydrogen concentration of the latter. Additional data is presented in /2/ for Zr-2.5Nb containing 200mg/kg hydrogen as radial hydrides. No HCC values are quoted, but the figure indicates that the transition for this material occurs over the range 260-280°C. It seems logical that with higher concentrations, larger hydrides will be present and thus it will be possible to initiate brittle fracture at higher temperatures. For this reason it is important to allow an adequate hold time at a test temperature for the hydrides to dissolve to the equilibrium concentration before performing a fracture toughness test.

Future investigations should examine the role of hydride platelet size and coarsness in more detail. It appears that this may be nearly as important in determining the transition behaviour as the specimen stress state. In addition, the effects of variations in hydride distribution through the tube wall are not yet known.

Since the mixed morphologies tested here had only minor effects on toughness, it would be desirable to test similar morphologies with higher HCC values. There is currently no information available on the transition behaviour of material having HCC values in the range 0.2-0.5.

6.2 Initiation Toughness

The results shown in Figure 6 show that the approach used here to define initiation toughness gives satisfactory results. The results are generally repeatable and show far less scatter than initiation values determined from potential drop records. These do not usually show clear inflections at initiation, and for ductile specimens, and are influenced by crack tip blunting and through-thickness yielding that often precedes true initiation. By taking the J value after 0.2mm of crack growth, these effects seem to be bypassed.

Problems could arise with this definition if the initiation data so defined is ever used in assessments of surface flaws in pressure tubes. In this case, 0.2mm represents a significant increase in flaw depth. The true initiation toughness is lower, and application of 0.2mm values could be non-conservative. This emphasizes the need to develop techniques for measuring radial fracture toughness for pressure tubes.

Some of the initiation toughness values given for the hydrided strip may be conservative. These are the specimens that fail in a brittle fashion but exhibit significant prior non-linearity in the load-displacement record. The initiation definition in ASTM E399, based on intersection of the curve by a secant at 95% of the initial slope, lies well below the instability value. Table 3 shows this for a number of the specimens in the transition region, from 240-280°C. However, since toughness in this region is unpredictable, the method is probably appropriate.

6.3 Geometry Effects

It should be noted that the upper shelf toughness level attained with the ductile specimens is largely dictated by the specimen size. The specimen size determines the maximum load that can be attained, termed the limit load or collapse load of the specimen. Once this load is reached, crack extension undergoes a transition from being "fracture mechanics" controlled to being determined by the global deformation of the specimen as its halves rotate about a plastic hinge /22/. The results in Table 3 show that all specimens exhibiting upper shelf behaviour have ratios of maximum load, P_{mv} to limit load, P_L, of about 1 or greater.

At some point after reaching maximum load, the J-R curve becomes dependent on the specimen geometry. Along with a loss in constraint, the specimen loses J-dominance, meaning that the crack tip stress strain field is no longer defined by J, or has deviated from the so-called HRR field. The ASTM test standards impose validity limits based on specimen size to define the limit of J-controlled growth. One of these is that the amount of stable crack extension should not exceed 10% of the initial ligament size, or about 0.8mm for the standard pressure tube C(T) specimen geometry. Examination of the data for ductile specimens indicates that maximum load occurs after about 0.6-1.0mm of stable crack growth. When C(T) specimen J-R curves are used for critical crack length (CCL) measurements, the point of tangency with the crack driving force (CDF) curve usually occurs at or beyond the maximum load point on the J-R curve, and thus in a region where the curve is geometry dependent. This has always been accepted in making CCL predictions for pressure tubes because the C(T) specimen has more constraint and should therefore produce a conservative J-R curve. Quantifying this conservatism is a major goal of the current pressure tube fracture research program.

It is important to consider what the differences in constraint between small specimens and pressure tubes will mean to the transition behaviour shown in these test results. It is expected that upper shelf toughness will be reached at lower temperatures in a tube. This could, however, be offset by irradiation strengthening of the material. So although COG-funded tests are currently underway to determine the effects of hydride morphology on fracture toughness in irradiated small specimens, future work should include tests on hydrided and irradiated tube sections.

ACKNOWLEDGEMENT

The author wishes to acknowledge the assistance of Mr. G.K. Shek and Mr. H. Seahra of the Materials Integrity Section for preparing the test materials. Mr. D.W. Carpenter and Mr. T.L. Zaban, a student, performed the fracture toughness tests. Mr. F. Smith of the Metallurgy section performed the scanning electron microscopy.

Recommended:

B. Mukherjee
Acting Section Head
Nondestructive and Fracture
Evaluation Section

Prepared:

A.C. Wallace
Engineer
Nondestructive and Fracture
Evaluation Section

Approved:

J. Brown
Manager
Metallurgical Research Department

REFERENCES

1. Coleman, C.E., Cheadle, B.A., Ambler, J.F.R., Lichtenberger, P.C. and Eadie, R.L. "Minimizing Hydride Cracking in Zirconium Alloys", Canadian Metallurgical Quarterly, Vol. 24, No. 3, pp. 245-250, 1985.

2. Simpson, L.A. and Chow, C.K.,"Effect of Metallurgical Variables and Temperature on the Fracture Toughness of Zirconium Alloy Pressure Tubes", Zirconium in the Nuclear Industry: Seventh International Symposium, ASTM STP 939, R.B. Adamson and L.F.P. Van Swam, Eds., American Society for Testing and Materials, Philadelphia, 1987, pp. 579-596.

3. Davies, P.H., Leger, M. and Shek, G.K., "Final Report: Reactivation of Orenda Burst Test Rig and Initial Testing of Two Zr-2.5wt%Nb Pressure Tubes", Ontario Hydro Research Division Report No. 83-265-K, August 16, 1983.

4. Davies, P.H. and Stearns, C.P., "Fracture Toughness Testing of Zircaloy-2 Pressure Tube Material with Radial Hydrides Using Direct Current Potential Drop", Fracture Mechanics: 17th Volume, ASTM STP 905, J.H. Underwood et. al., Eds., American Society for Testing and Materials, Philadelphia, 1986, pp. 379-400.

5. Lepik, O.E., Shek, G.K., Wallace, A.C., Stearns, C.P., and Seahra, H., The Effect of Hydride Morphology on the Axial Fracture Toughness of Zr-2.5Nb Pressure Tube Material, Ontario Hydro Research Division Report No. 86-93-K, July 15, 1986.

6. Leger, M., Shek, G.K., Donner, A. and Vesely, P.G. "OHRD Metallurgical Investigation of Pressure Tubes Removed from Pickering 'B' Unit 8", Ontarion Hydro Research Division Report No. 85-293-K, October 8, 1985.

7. Cheadle, B.A., "Interim Report of the Metallurgical Examination of the X-14 East End Fitting Assembly Removed from Bruce Unit 2", Atomic Energy of Canada Limited Report CRNL-2391, Chalk River Nuclear Laboratories, Chalk River, Ontario K0J 1J0, June, 1982.

8. Julien, M., Donner, A. and Leger, M., "The Occurence of Hydride Depleted Zones in Zr-2.5wt%Nb Pressure Tube Material", Ontario Hydro Research Division Report No. 79-520-K, December 5, 1979.

9. Bell, L.G. and Duncan, R.G., Atomic Energy of Canada Limited Report No. AECL-5110, Whiteshell Nuclear Research Establishment, Pinawa, Manitoba R0E 1L0, June 1975.

10. Chow, C.K., Davies, P.H., Coleman, C.E. and Simpson, L.A., Fracture Toughness of Zr-2.5 wt% Nb Pressure Tube From Pickering NGS-3 Fuel Channel J-09, Atomic Energy of Canada Limited Report WNRE-712, Whiteshell Nuclear Research Establishment, Pinawa, Manitoba R0E 1L0, 1986 May.

11. Chow, C.K. and Simpson, L.A., "Determination of Toughness of Irradiated Reactor Pressure Tubes Using Curved Compact Specimens", Fracture Mechanics: 18th Symposium, ASTM STP 945, D.T. Read and R.P. Reed, Eds., American Society for Testing and Materials, Philadelphia, 1988, pp. 419-439.

12. Newman, J.C., Jr., "Stress Analysis of the Compact Specimen Including the Effects of Pin Loading," Fracture Analysis, ASTM STP 560, American Society for Testing and Materials, 1974, pp. 105-121.

13. Simpson, L.A. and Clarke, C.F., "An Elastic-Plastic R-Curve Description of Fracture in Zr-2.5Nb Pressure Tube Alloy", Elastic_Plastic Fracture, ASTM STP 668, J.D. Landes et. al., Eds., American Society for Testing and Materials, Philadelphia, 1979, pp. 643-662.

14. Ells, C.E., Cheadle, B.A., Coleman, C.E. and Van der Kuur, J.H., "The Decomposition of Hydrides in Zirconium Alloys", Proceedings of Third International Congress on Hydrogen and Materials, Paris, June 7-11, 1982 (Atomic Energy of Canada Limited Report AECL-7711).

15. Kiefner, J.F., Maxey, W.A., Eiber, R.J. and Duffy, A.R., "Failure Stress Levels of Flaws in Pressurized Cylinders", Progress in Flaw Growth and Fracture Toughness Testing, ASTM STP 536, American Society for Testing and Materials, Philadelphia, 1973, pp. 461-481.

16. Simpson, L.A., "The Application of Ductile-Fracture Analysis to Predictions of Pressure Tube Failure", Atomic Energy of Canada Report No. AECL-6504, Whiteshell Nuclear Research Establishment, Pinawa, Manitoba R0E 1L0, August, 1981.

17. Kumar, V., German, M.D. and Shih, C.F., "An Engineering Approach for Elastic-Plastic Fracture Analysis", Topical Report EPRI-1931, Research Project 1237-1, Electric Power Research Institute, Palo Alto, California 94304, July, 1981.

18. Simpson, L.A., Ellis, R.B., Stark, D.J. and Shillinglaw, A.J., "The Effect of Irradiation and Irradiation Temperature on the Fracture Toughness of Cold-Worked Zr-2.5wt%Nb", Atomic Energy of Canada Limited Report No. AECL-8368, Whiteshell Nuclear Research Establishment, Pinawa, Manitoba R0E 1L0, September, 1984.

19. Wallace, A.C., Shek, G.K. and Lepik, O.E., "Effects of Hydride Morphology on Zr-2.5Nb Fracture Toughness", Zirconium in the Nuclear Industry: Eighth Symposium, ASTM STP 1023, L.F.P. Van Swam and C.M. Eucken, Eds., American Society for Testing and Materials, Philadelphia, 1989, pp. 66-88.

20. Simpson, L.A., Metallurgical Transactions, Vol. 12A, 1981, pp. 2113-2124.

21. Puls, M.P., Metallurgical Transactions, Vol. 19A, 1988, pp. 1507-1522.

22. Hu, J.M. and Albrecht, P., "Deformation Behaviour During Plastic Fracture of C(T) Specimen", presented at Second ASTM Symposium on User Experience with Elastic-Plastic Fracture Test Methods, Orlando, Florida, November 8-9, 1989.